BULLETIN OF THE POLISH ACADEMY OF SCIENCES
TECHNICAL SCIENCES, Vol. 69(5), 2021, Article number: e138813
DOI: 10.24425/bpasts.2021.138813

Topology algorithm built as an automaton with flexible rules

Katarzyna TAJS-ZIELIŃSKA* **and Bogdan BOCHENEK**

Faculty of Mechanical Engineering, Cracow University of Technology, Al. Jana Pawła II 37, 31-864 Kraków, Poland

Abstract. Developing novel methods, approaches and computational techniques is essential for solving efficiently more and more demanding up-to-date engineering problems. Designing durable, light and eco-friendly structures starts at the conceptual stage, where new efficient design and optimization tools need to be implemented. Nowadays, apart from the traditional gradient-based methods applied to optimal structural and material design, innovative techniques based on versatile heuristic concepts, like for example Cellular Automata, are implemented. Cellular Automata are built to represent mechanical systems where the special local update rules are implemented to mimic the performance of complex systems. This paper presents a novel concept of flexible Cellular Automata rules and their implementation into topology optimization process. Despite a few decades of development, topology optimization still remains one of the most important research fields within the area of structural and material design. One can notice novel ideas and formulations as well as new fields of their implementation. What stimulates that progress is that the researcher community continuously works on innovative and efficient topology optimization methods and algorithms. The proposed algorithm combined with an efficient analysis system ANSYS offers a fast convergence of the topology generation process and allows obtaining well-defined final topologies.

Key words: topology optimization; cellular automaton; flexible update rules.

1. INTRODUCTION

Simultaneously with the development of novel ideas and formulations within the topology optimization area, the implementation of topology optimization algorithms into engineering practice can be observed. This practical aspect of topology optimization becomes one of the most important issues of contemporary design. It stimulates research progress within groups working on efficient topology optimization algorithms. As a result, apart from traditional gradient methods based on the calculation of sensitivities of design variables applied to mathematical models, e.g. [1–4], there have been various non-gradient approaches proposed including efficient heuristic techniques. From the wide range of optimal topologies generators, one can point out ESO/BESO evolutionary structural optimization, e.g. [5–7], genetic algorithms, e.g. [8, 9], other biologically inspired algorithms, e.g. [10–12], material cloud method, e.g. [13], spline-based topology optimization, e.g. [14], level set method, e.g. [15, 16], proportional topology optimization [17], or moving morphable components approach, e.g. [18], among other things.

Novel and efficient heuristic optimization techniques inspired by biological, physical, or chemical phenomena (see [19–22]) are becoming increasingly popular within the research community and nowadays they are becoming more often an alternative to traditional approaches. Three aspects are raised here in favor of these techniques, namely: there is no need to calculate gradients; numerical implementation is relatively easy; any finite element code of structural analysis can be linked with such an algorithm.

Among techniques based on versatile heuristic concepts, one can choose Cellular Automata. Since the late 1940s, when von Neumann [23] and Ulam [24] proposed the concept of Cellular Automata, this idea has been of interest to the researchers representing various fields like social sciences, biology, physics, transport, or engineering science. Cellular Automata are built to represent the behavior of complicated systems in a relatively easy way. Special local rules are implemented to mimic the system performance. Hence, thanks to updating local rules in sequence, local physical quantities are updated respectively, which allows us to describe the global behavior of the system.

Over the years, Cellular Automata have been found appropriate for the description of different physical phenomena like, in particular, diffusion of gases [25], turbulence [26], or growth of crystals [27]. One can also find applications of Cellular Automata in computer science where, for instance, image analysis [28] and computer graphics can be pointed out.

Inou et al. proposed in [29, 30] to apply Cellular Automata to structural design and it was probably for the first time when topology optimization was discussed within the CA approach. Slightly later, similar ideas were also described in [31–33]. Since then many papers have been published on that subject. The majority of them have appeared during the last two decades, see [34–39], for example.

Tovar and co-workers have published a series of papers regarding the implementation of Cellular Automata rules inspired by the phenomenon of functional adaptation observed in bones [40–42]. An efficient CA algorithm was also proposed

*e-mail: Katarzyna.Tajs-Zielinska@pk.edu.pl

Manuscript submitted 2021-01-26, revised 2021-06-28, initially accepted for publication 2021-08-16, published in October 2021

and then developed by Bochenek and Tajs-Zielińska [43–46].

This paper takes a step further and presents a novel concept of flexible Cellular Automata rules and their implementation into structural topology optimization. The proposed CA approach applied to topology optimization offers a fast convergence of the topology generation process and allows us to obtain final topologies without the so-called grey-scale and checkerboard effects. Some plane and spatial structures have been selected to illustrate the effectiveness of the implementation of the Flexible Cellular Automata (FCA) topology algorithm for structure compliance optimization.

The outline of the paper is as follows. In Section 2, the topology optimization problem is formulated. The concept of Cellular Automata with flexible rules is introduced in Section 3, together with a detailed description of a numerical algorithm built based on this idea. Original introductory examples discussed in Section 4 illustrate the implementation of flexible rules in the topology generation process. Next, utilizing the results of the preliminary analysis, the Cellular Automaton is combined with ANSYS as an efficient structural analysis tool and in Sections 5 and 6, its application to selected, both plane and spatial, engineering tasks is presented. To cover a broad area of implementations, the discussed tasks include irregular cell lattice adding multiple load cases. Based on the results of the performed tests, the paper ends with concluding remarks and with some recommendations for the potential users.

2. OPTIMIZATION OF STRUCTURAL TOPOLOGY

Research within the topology optimization area has been already conducted for a few decades and the results have been widely presented in engineering literature on structural and material design. The papers by Bendsoe and Kikuchi [47] and Bendsoe [1], dating back to the late 1990s, are broadly treated as pioneering ones. Since then, numerous approaches to the generation of optimal topology have been presented. Emerging concepts have been applied to various engineering and research fields. Among them, one can find heat transfer problems, e.g. [48], aeronautical industry, e.g. [49], through civil engineering, e.g. [50], mechanical engineering, e.g. [51] and architecture, e.g. [47, 48, 52, 53] to material science, e.g. [54, 55]. A broad discussion on various aspects of topology optimization has been provided by many survey papers and books, e.g. [56–59]. The spectrum of numerous applications of topology optimization ranges from classic Michell trusses to sophisticated contemporary engineering structures. The remarkable progress within the topology optimization field would not be possible without versatile, innovative, and efficient methods and algorithms. The important issue nowadays becomes the possibility of an easy combination of the developed algorithms with structural analysis solvers built on the finite element method.

The idea of performing topology optimization for a specified design domain is to generate a material layout within this domain to meet the assumed optimality criteria. The optimized structure gains a new shape and material layout since some parts of the material are relocated and others are selectively removed. It allows us to create, for example, a stiffer construction with a minimal amount of material. Concept solutions generated this way can be an inspiration for further efforts of engineers and designers.

Structural topology optimization problems are usually formulated as compliance-based or stress-constrained approaches. Various formulations are discussed for which the compliance or weight are mainly chosen as objectives whereas volume fraction often plays the role of a constraint. As for the stress-based approaches, one can pay attention, for example, to the recent papers [60–62].

The most commonly analyzed structural topology optimization problem is to generate within a design domain material layout which leads to a minimal value of the structure compliance c, the equation (1). The finite element approach has been applied. The available material volume fraction κ is defined and treated as the constraint imposed on structure volume V in the optimization process, the equation (2).

$$\min \quad c(\mathbf{d}) = \mathbf{u}^T \mathbf{k}\ \mathbf{u} = \sum_{n=1}^{N} d_n^p \mathbf{u}_n^T \mathbf{k}_n \mathbf{u}_n\,, \tag{1}$$

$$\text{subject to} \quad V(\mathbf{d}) = \kappa V_0\,, \tag{2}$$

$$\mathbf{k}\,\mathbf{u} = \mathbf{f}, \tag{3}$$

$$0 < d_{\min} \leq d_n \leq 1. \tag{4}$$

The quantity $\mathbf{u}_n$ represents a displacement vector whereas $\mathbf{k}_n$ stands for the stiffness matrix. Both are defined for N elements. The design variable d_n, which represents the material relative density, is assigned to each element. In the equation (3), $\mathbf{k}$ is the global stiffness matrix, $\mathbf{u}$ stands for the global displacement vector and $\boldsymbol{f}$ represents a vector of forces. Singularity in the equation (4) is avoided due to the simple bounds imposed on the design variables with $d_{\min}$ as a non-zero minimal value of a relative density.

As to the material representation, SIMP, solid isotropic material with penalization (e.g. [56]) in the form of a power law, is adapted. For each finite element, the modulus of elasticity E_n is a function of the design variable d_n.

$$E_n = d_n^p E_0\,, \quad \rho_n = d_n \rho_0\,. \tag{5}$$

In the equation (5), p (typically $p = 3$) is responsible for the penalization of intermediate densities, which facilitates controlling the design process and leads to obtaining black-and-white resulting structures. The quantities E_0 and ρ_0 stand for the modulus of elasticity and material density, both defined for solid material. The process of topology generation leads to a redistribution of the material within the design domain, which results in removing parts unnecessary from the design criteria point of view.

3. FLEXIBLE RULES OF CELLULAR AUTOMATA

While performing the analysis and topology optimization, the design domain is decomposed into a lattice of cells which are

usually equivalent to finite elements. Cellular Automata allow us to mimic physical systems performance by implementing simple local rules, which govern local interactions between the neighboring cells. Based on local information gathered within neighboring cells, a complex problem can be replaced by a sequence of simple decisions. Identical rules are applied to all cells simultaneously. The two schemes can be adapted to cell states updating, i.e. the Gauss-Seidel update rule, where already modified values obtained for cell neighbors in the current iteration are taken into account or the Jacobi update scheme, for which states of neighboring cells determined in the previous iteration are the basis for the updating process.

Because all cells have the same neighborhood, for the ones situated at the boundary, the neighboring cells lay outside the feasible domain. It is necessary from the topology optimization point of view to specify and assign design variables values to them. One can choose from periodic, reflecting, adiabatic, or specified boundary conditions. The latter option is implemented in this paper and to all cells lying outside the design domain zero is assigned as the design variable value.

The original heuristic local update rule utilizing the Jacobi update scheme has been proposed in [43], see the equations (6), (7):

$$d_n^{new} = d_n + \Delta d_n, \tag{6}$$

where

$$\Delta d_n = \left[a_0 \alpha_n + \sum_{k=1}^{M} \alpha_k \right] \frac{m}{M+1}. \tag{7}$$

In the equation (7), the quantity m plays the role of admissible change of the design variable values. The multiplier a_0 allows us to modify the value of the component associated with a central cell, as compared to the components assigned to M neighboring cells, usually $a_0 = 1$:

$$\alpha_n = \begin{cases} -C_\alpha & \text{if } c_n \le c^*, \\ C_\alpha & \text{if } c_n > c^*. \end{cases} \tag{8}$$

In the equation (8), c_n refers to the local compliance associated with cell n, c^* stands for a threshold value and C_α is a constant value assigned to each cell. Depending on the result of the selection controlled by the equation (8) material is added to or removed from the cell n.

It is worth noting that, alternatively, instead of threshold compliance value the threshold number of cells can be considered. To do this, the cell compliances are sorted in ascending order and consecutive indices are ascribed to the sorted cells. In what follows c can be replaced now by N and the equation (8) can be rewritten in the form of the equation (9):

$$\alpha_n = \begin{cases} -C_\alpha & \text{if } n \le N^*, \\ C_\alpha & \text{if } n > N^*. \end{cases} \tag{9}$$

In this paper, a modification of these rules is proposed. Namely, to make local rules more flexible, instead of one threshold value N^*, two values N_1 and N_2 are introduced. The structural analysis is performed first and, based on the obtained results, the values of local compliances are calculated for all cells/elements. Then, compliances are sorted in ascending order, and those having the lowest and the highest values are identified. Having finished that, N_1, N_2 are selected and $F(n) = -C_\alpha$ if $n < N_1$ and $F(n) = C_\alpha$ if $n > N_2$ are assigned. As to the intermediate interval $N_1 \le n \le N_2$, it is proposed to introduce a special monotonically increasing function representing element compliances and then assign the values to the design elements, respectively:

$$F(n) = \begin{cases} -C_\alpha & \text{if } n < N_1, \\ f(n) & \text{if } N_1 \le n \le N_2, \\ C_\alpha & \text{if } n > N_2. \end{cases} \tag{10}$$

The update rule takes now the following form:

$$\Delta d_n = \left[a_0 F(n) + \sum_{k=1}^{M} F(k) \right] \frac{m}{M+1}, \tag{11}$$

where α_n from the equation (9) has been here replaced by $F(n)$. In the proposed formulation, the CA algorithm performance is influenced by the choice of $f(n)$. Here, the function of n presented below has been adapted:

$$f(n) = C_\alpha \frac{\tanh\left[\beta\left(\frac{n-N_1}{N_2-N_1} - \frac{1}{2}\right)\right]}{\tanh\left(\frac{1}{2}\beta\right)}. \tag{12}$$

The parameter β decides about the form of the $f(n)$ function. In what follows for β tending to zero, $f(n)$ tends to a linear function, whereas for large values of β, $f(n)$ tends to a step function, see Fig. 1. One can observe that the first case refers to the linear representation of sorted compliances as proposed in [63], whereas the step function case denotes the original version of the CA algorithm as presented in [43]. This paper focuses on the intermediate values of β. Adjusting β values influences the algorithm performance ensuring the flexibility of update rules.

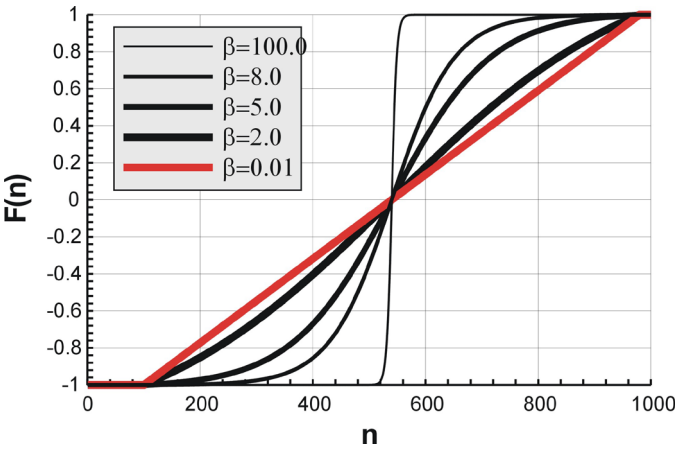

Fig. 1. Function $F(n)$ for selected values of β

3.1. Implementation of irregular lattices

The proposed flexible CA rules can be easily adjusted to the case when the lattice of cells is irregular. Such lattices are implemented mostly when a design domain is highly irregular and covering the domain with uniform, usually regular, cells may be difficult or even impossible. The advantage of introducing an unstructured cell layout can be visible also when the structure geometry includes sharp edges or holes, which are the sources of stress concentration. In such cases, the regions of stress intensity should be covered with a fine mesh, whereas for the rest of the structure regular mesh remains sufficient. The main advantage regarding the implementation of a non-uniform layout of cells/mesh is that it allows us to obtain an accurate solution without increasing the number of cells necessary if one wants to cover the whole structure with the fine mesh. From the numerical point of view, it is important to underline that the non-uniform layout of cells can be related to the finite element mesh, although not necessarily. Along with the implementation of irregular mesh, the local Cellular Automata rules have to be reformulated taking into account the sizes of the neighboring cells or the lengths of mutual boundaries. These aspects influence the relations between the central cell and its neighbors. Considering the above, it is proposed to modify the rule update according to the following:

$$\Delta d_n = \left[a_0 F(n) \frac{A_n}{A} + \sum_{k=1}^{M} F(k) \frac{A_k}{A} \right] \frac{m}{M+1}, \tag{13}$$

where

$$A = A_n + \sum_{k=1}^{M} A_k . \tag{14}$$

In the equations (13)-(14), A_n denotes the area of the n-th cell whereas A stands for the area of the n-th cell neighborhood.

3.2. The numerical algorithm in use

The implementation of the local CA rules proposed above requires a numerical algorithm to be developed. In what follows, the FCA algorithm was built. A sequential approach was chosen which means that the structural analysis performed for each iteration is followed by the application of the local update rules. Simultaneously, in each iteration, the volume constraint is applied for the updated design elements. Therefore, the generated topology preserves a defined volume fraction of the solid material that allows us to keep this fraction constant during the optimization procedure. As to the neighborhood, either the von Neumann type one (the neighboring cells share common edges with the central cell) or the Moore type one (the neighboring cells share common vertices with the central cell) was adopted. The assumed change of the objective function value for subsequent iterations was implemented as the stopping criterion, but in general, it can be defined also as performing a selected number of iterations.

The topology generation was performed using the in-house code written in Matlab for introductory examples, whereas for engineering problems an optimization module was linked to a professional system ANSYS, which is responsible for performing structural analyses.

To control the effectiveness of the proposed basic concept, the implementation of the adaptive technique is suggested.

Therefore, the threshold values N_1 and N_2 can be adjusted so that the width of the interval $[N_1, N_2]$ can be modified during the iteration process. The leading idea while working on the strategy of adjusting $[N_1, N_2]$ interval is to find the preliminary layout first (the exploration phase) and then to drive the solution to a distinct solid/void structure (the exploitation phase). Then, one starts with a relatively wide initial interval $[N_1, N_2]$ and successively reduces the interval width. It means that at the beginning the Automaton searches the large design domain and preliminarily outlines the structure layout by eliminating void cells. As the iterative process continues, a temporary solution is tuned. Tuning by subsequently reducing interval $[N_1, N_2]$ width leads to eliminating the cells/elements of intermediate density, the so-called grey ones, and finally leads to a distinct solid/void structure. The abovementioned strategy of tightening the search domain resembles the one which is known from the simulated annealing process. The described strategy results in modifying the shape of the $F(n)$ function, which is illustrated in Fig. 2.

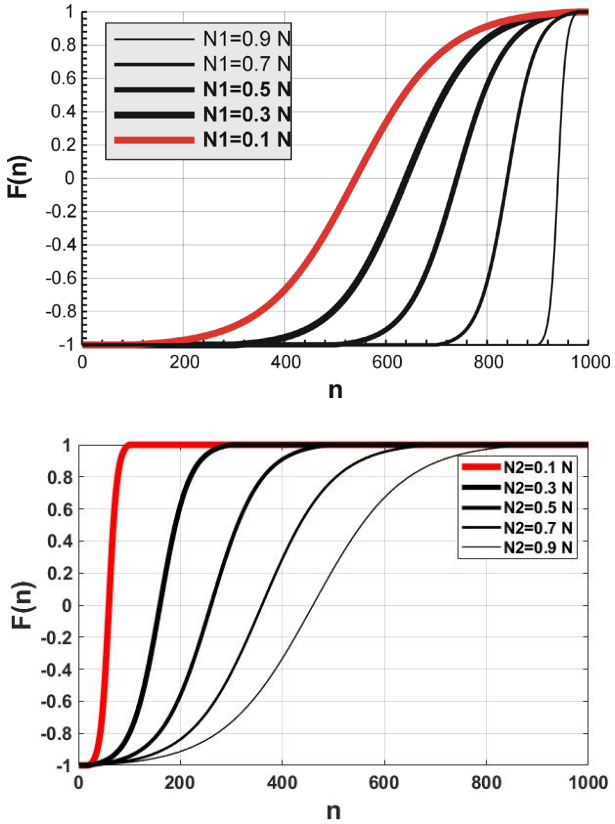

Fig. 2. Function $F(n)$ implementation based on N_1, $N_2 = 0.98$ N (above) or N_2, $N_1 = 0.02$ N (below)

3.3. The algorithm performance in detail

In this section, the performance of the numerical algorithm is discussed in detail. Two basic structures considered earlier in [43] were chosen to illustrate the topology generation pro-

cess. It allows us to link the discussion in this section to the approach presented in [43].

The square structure shown in Fig. 3 is considered first.

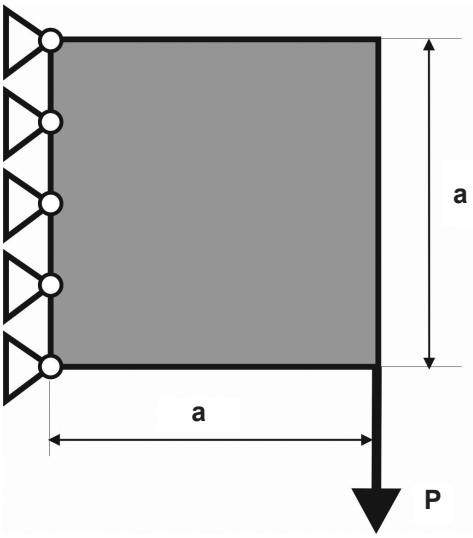

Fig. 3. The initial structure with applied load and support (basic structure 1

The mesh of 1600 (40×40) square elements was generated to perform structural analysis and topology optimization for the data: load $P = 100$ N, $a = 4$ m, the Young modulus $E = 20$ GPa, and the Poisson ratio $\nu = 0.3$. As reported in [43], the compliance found for this structure for the volume fraction 0.5 equals $1.04 \cdot 10^{-6}$ Nm.

Now, the approach proposed in the present paper is applied. The strategy of $F(n)$ implementation is as follows: one starts with $N_1 = N \cdot 0.3$ and then for $it > 25$ $N_1 = N \cdot 0.5$, for $it > 50$ $N_1 = N \cdot 0.7$ and for $it > 75$ $N_1 = N \cdot 0.9$, where N is the total number of elements. $N_2 = N \cdot 0.98$ remains unchanged for the whole iteration process. The Moore-type neighborhood is applied.

The FCA algorithm found the final topology for $\beta = 1.5$, see Table 1. In Fig. 4, the final topology obtained, together with the iteration history in Fig. 5, are shown. The value of compliance for the obtained result equals $1.0335 \cdot 10^{-6}$ Nm.

The number of iterations which refers to 1% and (0.01%) change of the objective function value for subsequent iterations

Table 1

The values of compliance [10^{-6} Nm] obtained while implementing the FCA algorithm for various values of β

β	0.1	1.0	1.5	2.0
Compl.	1.0343	1.0370	**1.0335**	1.0339
Iter.	13 (35)	13 (38)	13 (38)	12 (38)

β	3.0	4.0	5.0	6.0
Compl.	1.0339	1.0356	1.0382	1.0427
Iter.	11 (39)	11 (39)	10 (39)	10 (37)

Fig. 4. The final topology

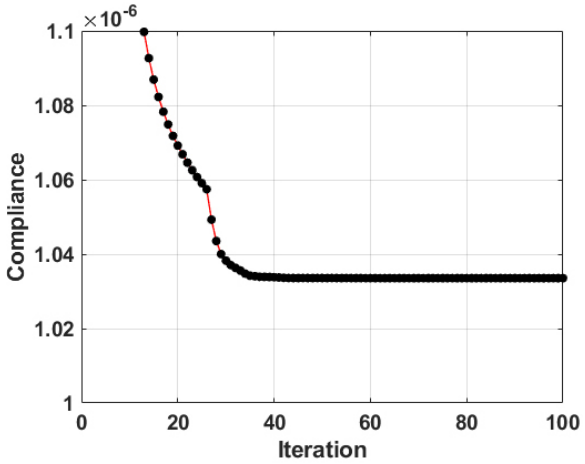

Fig. 5. Results: Compliance history

is given in the third row of Table 1. The final topology obtained for $\beta = 1.5$ is presented in Fig. 4.

In Fig. 5, the history of 100 iterations is illustrated. A sharp change in the objective function values is related to the implemented strategy, namely the flexibility of update rule was activated, the interval $[N_1, N_2]$ was reduced, and this caused significant changes of the design variables values. It is worth emphasizing that this feature can be observed also for other examples discussed in the subsequent sections of the paper.

The comparison of the solutions obtained for the selected values of β is presented in Fig. 6. As can be seen from this picture, only slight differences between the topologies are observed.

Moreover, for comparison, the $N_1 = N_2 = N^*$ strategy is implemented: one starts with $N^* = N \cdot 0.3$ and then for $it > 25$ $N^* = N \cdot 0.5$, for $it > 50$ $N^* = N \cdot 0.7$ and for $it > 75$ $N^* = N \cdot 0.9$, where N is the total number of elements. The compliance for the obtained topology, presented in Fig. 7, is equal to $1.0411 \cdot 10^{-6}$ Nm.

In Fig. 8 the history of 100 iterations is illustrated.

The rectangular structure shown in Fig. 9 is discussed next.

The mesh of 3200 (80×40) square elements is generated to perform structural analysis and topology optimization for the data: load $P = 100$ N, $a = 40$ mm, the Young modulus $E = 10$ GPa, and the Poisson ratio $\nu = 0.3$. As reported in [43], the compliance value, found for this structure for the volume fraction 0.5, equals 14.04 Nmm.

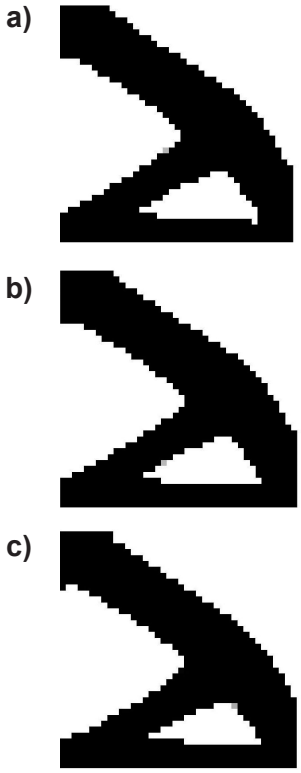

Fig. 6. The comparison of the solutions obtained for different values of β: 0.1 (a), 1.5 (b), 5 (c)

Fig. 7. The final topology

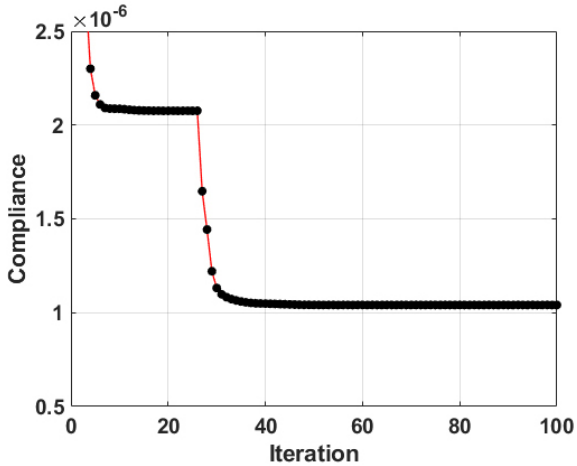

Fig. 8. Results: Compliance history

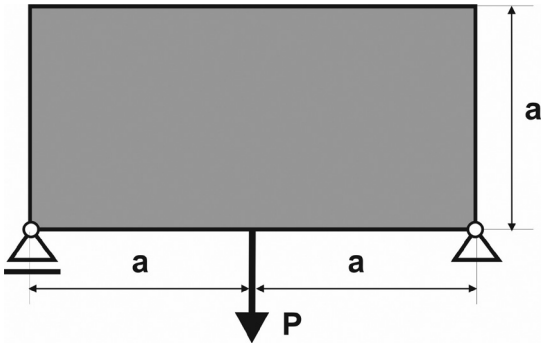

Fig. 9. The initial structure with applied loads and supports (basic structure 2)

As for the strategy of $F(n)$ implementation, one starts with $N_1 = N \cdot 0.02$ and then for $it > 15$ $N_1 = N \cdot 0.5$ and for $it > 30$ $N_1 = N \cdot 0.55$, where N is the total number of elements. $N_2 = N \cdot 0.6$ remains unchanged for the whole iteration process. The Moore-type neighborhood was applied.

The FCA algorithm found the final topology for $\beta = 4$, see Table 2. In Fig. 10, the final topology obtained, together with the iteration history in Fig. 11, are shown. The value of compliance for the obtained result equals 13.930 Nmm.

Table 2
The values of compliance [Nmm] obtained while implementing the FCA algorithm for various values of β

β	0.1	1.0	2.0	3.0
Compl.	13.952	13.953	13.956	13.942
Iter.	15 (42)	15 (39)	14 (41)	13 (41)

β	4.0	5.0	6.0	7.0
Compl.	13.930	13.955	14.005	14.018
Iter.	12 (41)	11 (44)	10 (43)	10 (41)

Fig. 10. The final topology

The comparison of the solutions obtained for the selected values of β is presented in Fig. 12. As can be seen from this picture, only slight differences between the topologies are observed.

For comparison, the $N_1 = N_2 = N^*$ strategy was implemented: one starts with $N^* = N \cdot 0.25$ and then for $it > 15$ $N^* =$

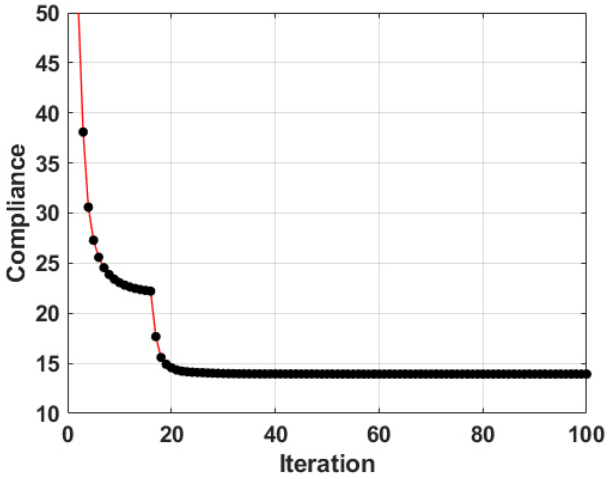

Fig. 11. Results: Compliance history

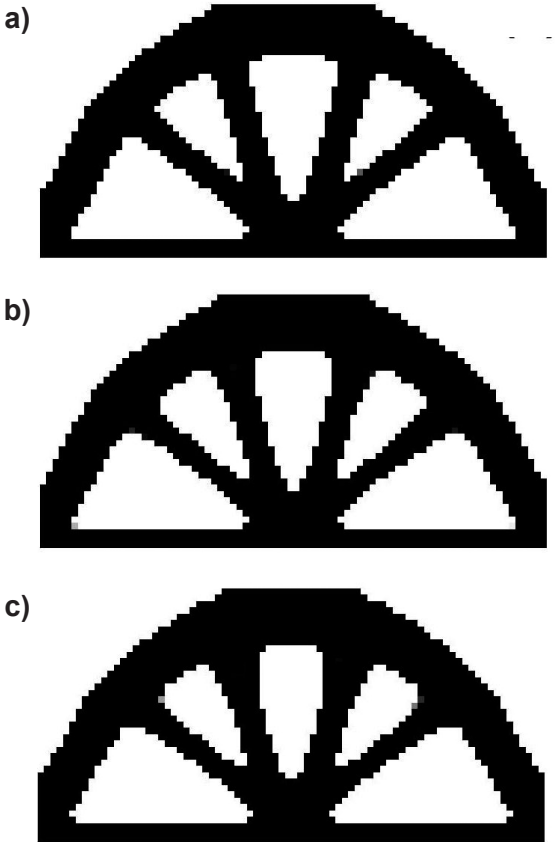

Fig. 12. The comparison of the solutions obtained for different values of β: 0.1 (a), 4 (b), 7 (c)

$N \cdot 0.5$ and for $it > 30\ N^* = N \cdot 0.7$, where N is the total number of elements. The compliance for the obtained topology, presented in Fig. 13, is equal to 14.021Nmm. In Fig. 14, the history of 100 iterations is illustrated.

It can be seen from the presentation of this section that due to the introduced flexibility of the update rules, the FCA algorithm allows us to obtain the results which can outperform the ones found in [43].

Fig. 13. The final topology

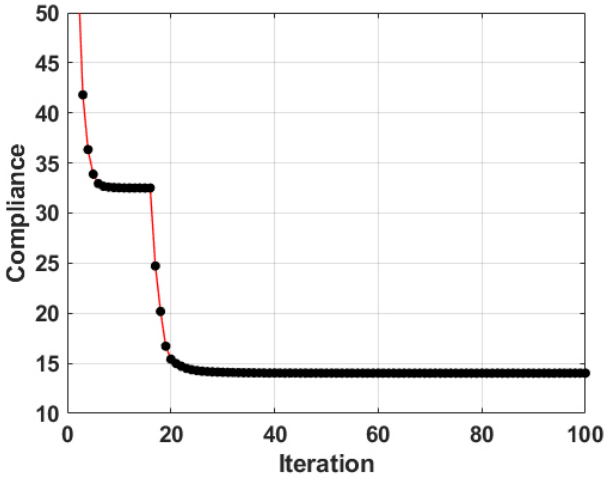

Fig. 14. Results: Compliance history

4. INTRODUCTORY EXAMPLES

To illustrate how the FCA algorithm works, a set of original introductory examples was proposed and detailed calculations were performed for them.

4.1. The bird-like test structure

The structure shown in Fig. 15 was selected as the first test example. The mesh of 6300 elements was generated to perform structural analysis and topology optimization. For: load $P = 50$ N, $a = 10$ mm, the Young modulus $E = 10$ GPa and the Poisson ratio $\nu = 0.3$, the FCA algorithm found the final

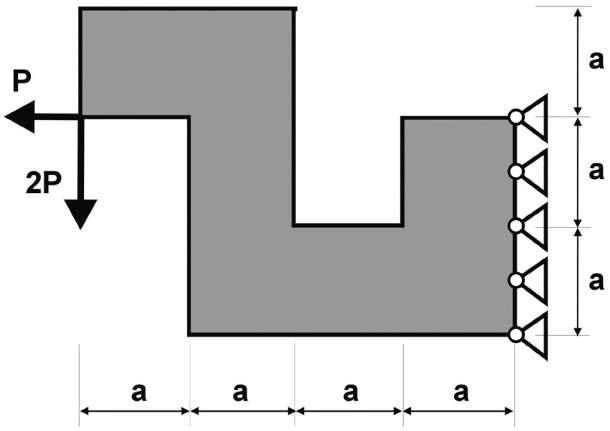

Fig. 15. Results: The final topology (test structure 1)

topology for $\beta = 4$. The Moore-type neighborhood was applied. In Fig. 16, the final topology obtained for the volume fraction 0.3 (concerning the initial rectangle 120×90) or 0.51 (with initial voids neglected), together with the iteration history in Fig. 17, are shown. The value of compliance for the obtained result equals 220.91 Nmm. To facilitate comparison, the compliances for various values of β are given in Table 3. The process of topology generation is illustrated in Fig. 18.

Fig. 16. Results: Compliance history

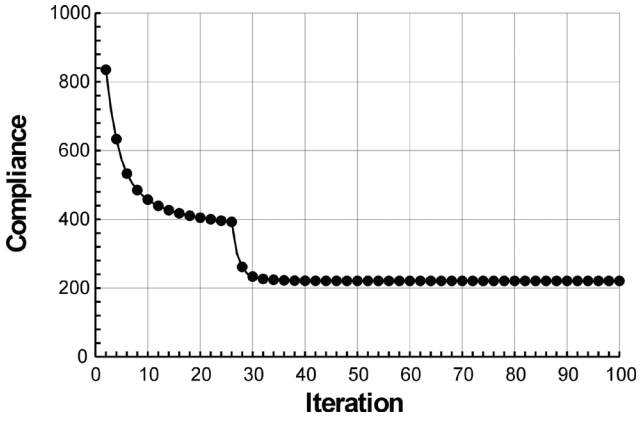

Fig. 17. Results: Compliance history (test structure 1)

Table 3

The values of compliance [Nmm] obtained while implementing the FCA algorithm for various values of β

β	0.1	1.0	2.0	3.0	4.0
Compl.	222.92	222.66	221.96	221.20	**220.91**
Iter.	18 (56)	18 (55)	18 (48)	18 (49)	17 (47)

β	5.0	6.0	7.0	8.0	$N_1 = N_2$
Compl.	221.57	222.58	224.13	225.36	229.97
Iter.	16 (47)	15 (48)	14 (51)	13 (47)	

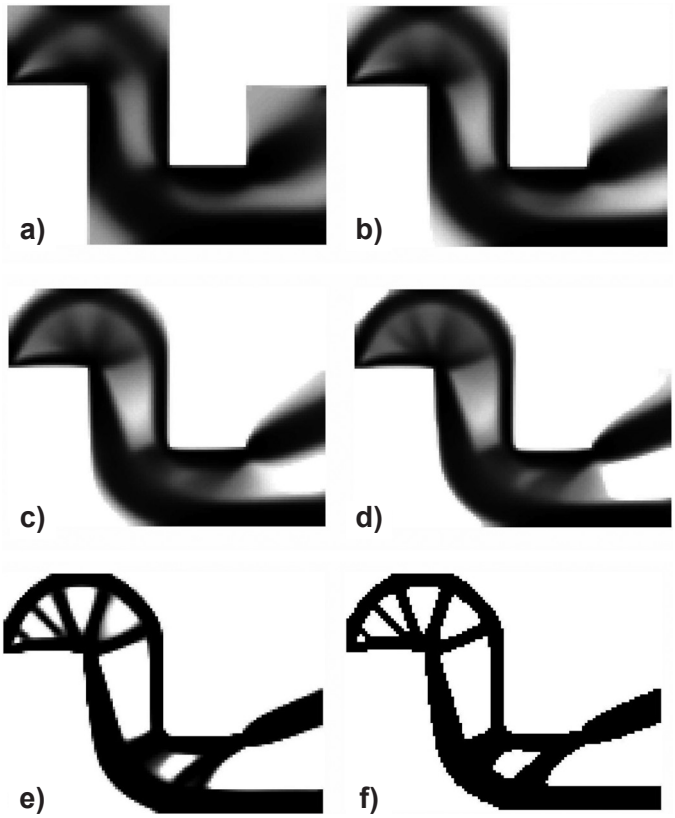

Fig. 18. An overview of the topology generation process. The middle topologies for iterations 2 (a), 4 (b), 10 (c), 20 (d), 30 (e) and 100 (f), respectively

The strategy of $F(n)$ implementation is as follows: one starts with $N_1 = N \cdot 0.02$ and then for $it > 25$ $N_1 = N \cdot 0.6$ and for $it > 50$ $N_1 = N \cdot 0.8$, where N is the total number of elements. $N_2 = N \cdot 0.98$ remains unchanged for the whole iteration process.

For comparison, the $N_1 = N_2 = N^*$ strategy has been implemented: one starts with $N^* = N \cdot 0.6$ and then for $it > 10$ $N^* = N \cdot 0.7$, for $it > 20$ $N^* = N \cdot 0.75$, for $it > 30$ $N^* = N \cdot 0.8$, for $it > 40$ $N^* = N \cdot 0.85$ and for $it > 50$ $N^* = N \cdot 0.9$, where N is the total number of elements.

4.2. The gripper-like test structure

The structure shown in Fig. 19 was proposed as test example 2. The value of applied load equals 50 N. The Young modulus $E = 10$ GPa and the Poisson ratio $\nu = 0.3$ stand for the material data. The volume fraction was selected as 0.35 (with respect to the initial rectangle 100×100) or 0.365 (with initial voids neglected), and parameter $a = 20$ mm. The regular mesh of 9600 elements was implemented. The Moore-type neighborhood was applied. The topology generation was performed and the resulting structure is presented in Fig. 20, while in Fig. 21, the history of 100 iterations is illustrated. For the final topology, compliance equal to 26.84 Nmm was found. This result was obtained for $\beta = 2$. To facilitate a comparison, the compliances for selected values of β are given in Table 4. Moreover, selected middle topologies and the final one obtained for the gripper structure are shown in Fig. 22.

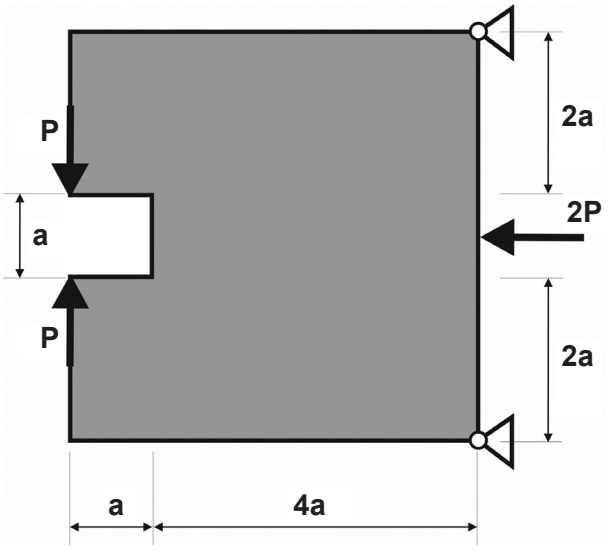

Fig. 19. An initial structure with applied loads and support (test structure 2)

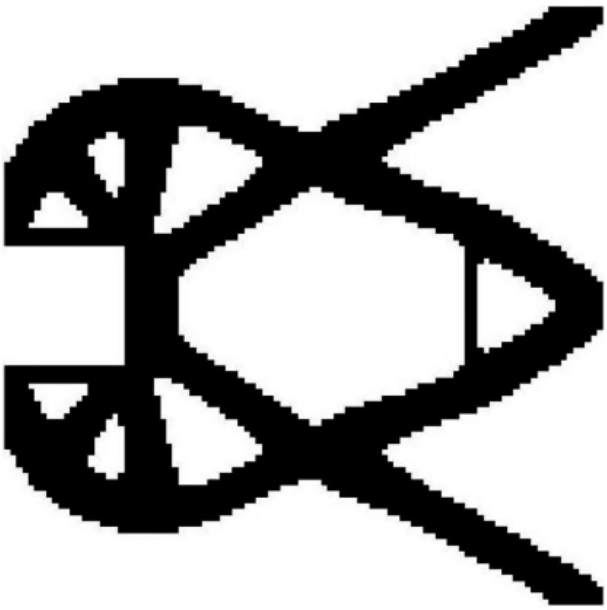

Fig. 20. Results: The final topology (test structure 2)

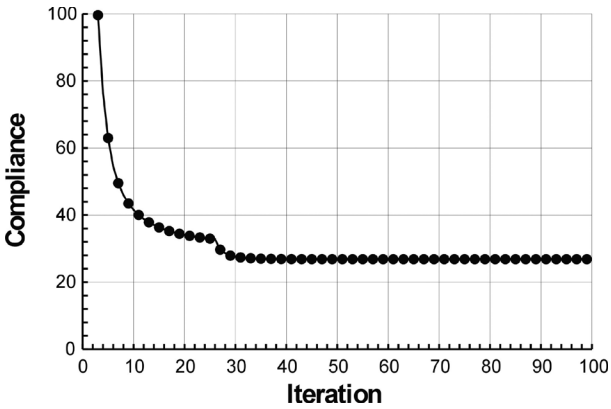

Fig. 21. Results: Compliance history (test structure 2)

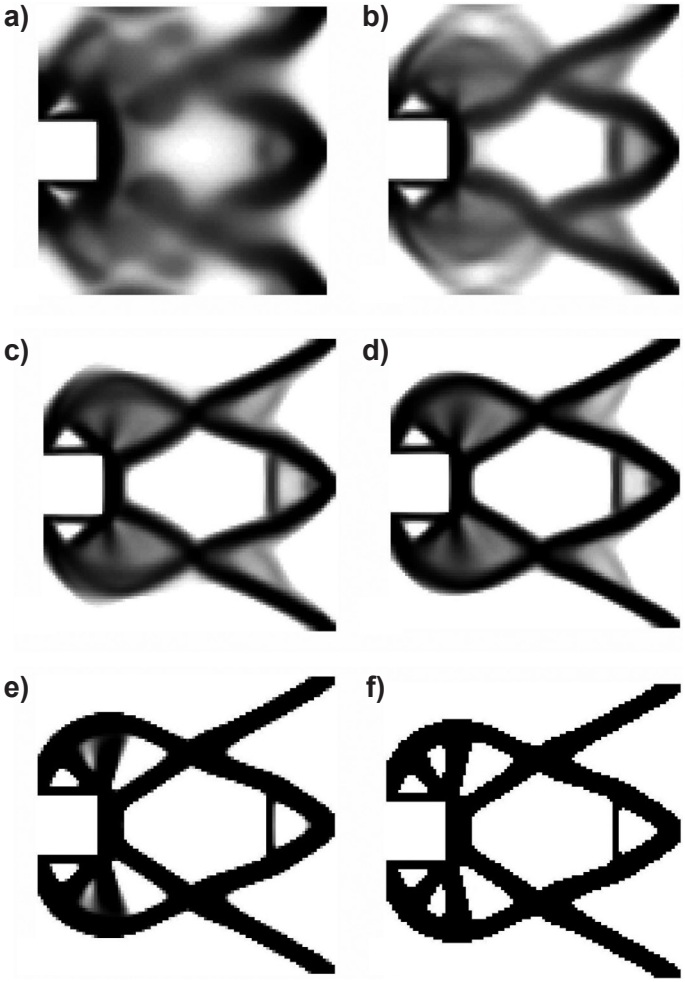

Fig. 22. An overview of the topology generation process. The middle topologies for iterations 2 (a), 4 (b), 10 (c), 20 (d), 30 (e) and 100 (f), respectively

Table 4

The values of compliance [Nmm] obtained while implementing the FCA algorithm for various values of β

β	0.1	1.0	2.0	3.0	4.0
Compl.	26.92	26.88	26.84	26.94	27.04
Iter.	20 (44)	20 (51)	20 (45)	20 (46)	20 (43)

β	5.0	6.0	7.0	8.0	$N_1 = N_2$
Compl.	27.07	27.09	27.11	27.19	29.48
Iter.	20 (46)	20 (47)	20 (45)	19 (50)	

The strategy of $F(n)$ implementation is the same as for the previous example.

The final topology obtained for the volume fraction 0.48 (with respect to the initial rectangle 100×100) or 0.50 (with initial voids neglected), is presented Fig. 23. The value of compliance for the obtained topology equals 21.063 Nmm. This result was obtained for $\beta = 1$.

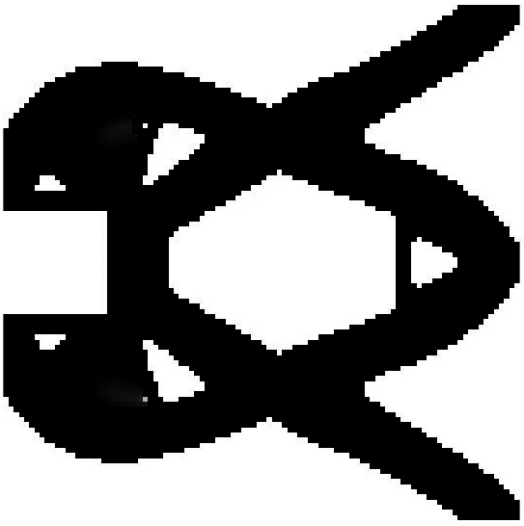

Fig. 23. Results: The final topology (test structure 2, volume fraction 0.5)

This paper aims to introduce the original idea of the FCA topology generator. The algorithm, which is based on flexible local rules, is the extension and generalization of formerly presented concepts. To sum up the results of the topology generation performed for the test structures, it is worth comparing them with the ones which can be found using other approaches. The well-recognized algorithm presented by Andreassen et al. [3] was chosen for this purpose. The results are shown in Table 5. It can be seen that the CA algorithm introduced in this paper allows us to find the results which can be better in terms of the objective function values.

Table 5
The algorithm effectiveness

Algorithm	Structure No 1	Structure No 2
FCA	220.91	26.84
Top88 [3]	220.40	27.59

5. PERFORMANCE IN 2D

To examine the effectiveness of the introduced concept of Cellular Automata topology generator, a series of illustrative examples including engineering ones was selected to show the algorithm performance. To show the versatility of the approach, both regular and irregular cell lattices are considered.

The proposed topology generator is versatile and can be easily combined with any solver built on the finite element method. Next, the optimization module was linked to the professional system ANSYS, which is responsible for performing structural analyses. It is worth noting that the proposed algorithm does not require additional density filtering, the so-called grey elements are eliminated and generated topologies are free from the checkerboard effect.

Based on numerical tests performed, including these considered in Sections 3.3 and 4, the following unified strategy of interval $[N_1, N_2]$ adjustment can be recommended: one starts with $N_1 = N \cdot 0.02$ and then for $it > 25$ $N_1 = N \cdot 0.5$, where N is the total number of cells/elements. $N_2 = N \cdot 0.98$ remains unchanged for the whole iteration process. The algorithm utilizes the Moore type of neighborhood for the examples of this section.

5.1. The mechanical part – an engineering example

The two-dimensional mechanical part presented in Fig. 24 was chosen as an example of an engineering structure. The Young modulus E of the employed linear, elastic, isotropic material equals 207.4 GPa, the Poisson ratio $\nu = 0.3$. Within the structure, the non-optimized region is shown in Fig. 25 as the blue area, whereas the design domain is presented as the red area. The regular grid of 17865 finite elements is adapted with the element edge length equal to 0.5 mm. As mentioned before, the ANSYS software was used as a static analysis tool with a two-dimensional 4-node element Plane42. The volume fraction was selected as 0.5. The concentrated forces are equal to 2000 N each and the distributed supports applied along the inner edge of left holes are shown in Fig. 25. The compliance for the initial structure equals 105.09 Nm, whereas the one for the final topology found for $\beta = 4$ is equal to 58.42 Nm. For comparison, Table 6 presents the values of final compliances obtained for different values of β. Figures 26 and 27 show he final topology and the iterations history, respectively.

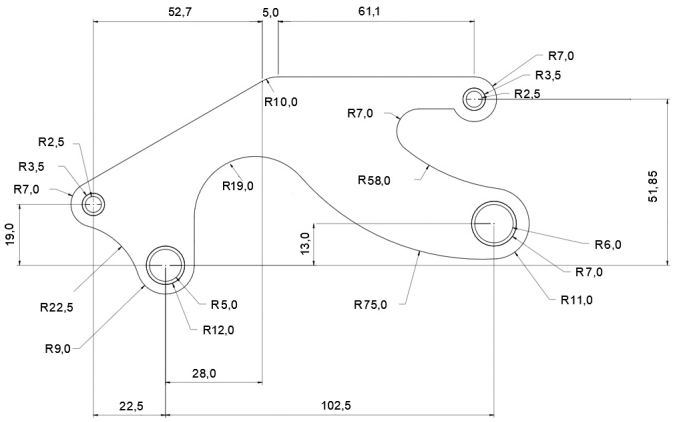

Fig. 24. The geometry of the structure

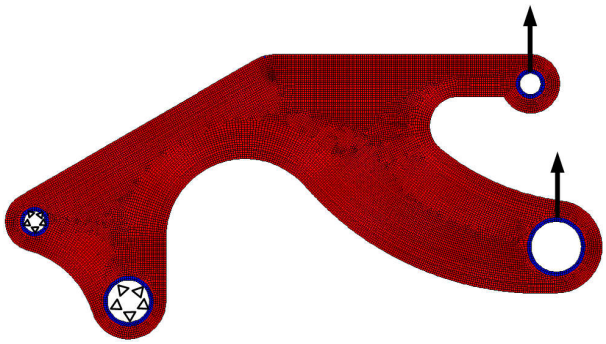

Fig. 25. Design domain, loads, and support

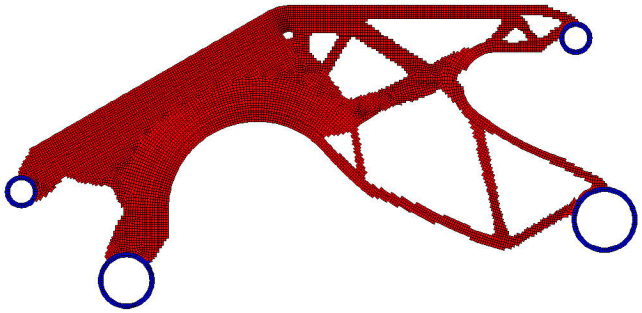

Fig. 26. Results: The final topology of the mechanical part

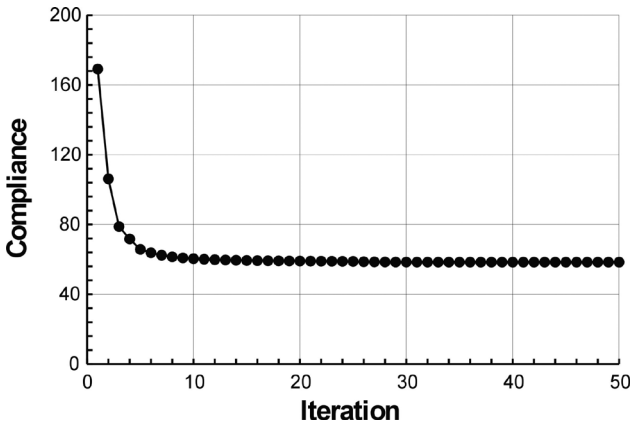

Fig. 27. Results: Compliance history for the mechanical part

Table 6
The values of compliance [Nm] obtained while implementing the FCA algorithm for various values of β

β	0.1	4.0	8.0
Compl.	58.66	58.42	58.68

5.2. The windmill structure – generation of topology for irregular lattice

As the numerical example of the efficiency of the method for the irregular lattice of finite elements, a two-dimensional windmill structure under torsion was selected. The structure is symmetric with respect to the vertical and horizontal axes. Two concentrated forces with an equal value of 1 kN are applied at the corners of the wings, two corners of the structure are supported as shown in Fig. 28. The irregular mesh of 9558 elements was applied, where the regions surrounding acting loads and inner corners are covered with finer mesh. It is worth underlining that to implement finer mesh for the whole structure, 50655 elements would be needed. The ANSYS software with a 4-node element Plane42 was used for static analysis. The element edge length for the coarse mesh was defined as 0.025 m, and then the refinement at the selected key points was implemented with the depth of the refinement equal to 3 and the minimal level of the refinement. The material data for this example are the Young modulus $E = 210$ GPa and the Poisson ratio $\nu = 0.3$ (material is linear, elastic, and isotropic). The volume fraction equals 0.5. The compliance value for the initial structure is equal to $7.381 \cdot 10^{-4}$ Nm. The optimization was performed and the generated final topology is shown in Fig. 29, whereas the iterations history is given in Fig. 30. The calculation of the compliance for the solution obtained for $\beta = 6$ gives $5.053\ 10^{-4}$ Nm. For comparison, Table 7 presents values of final compliances obtained for different values of β.

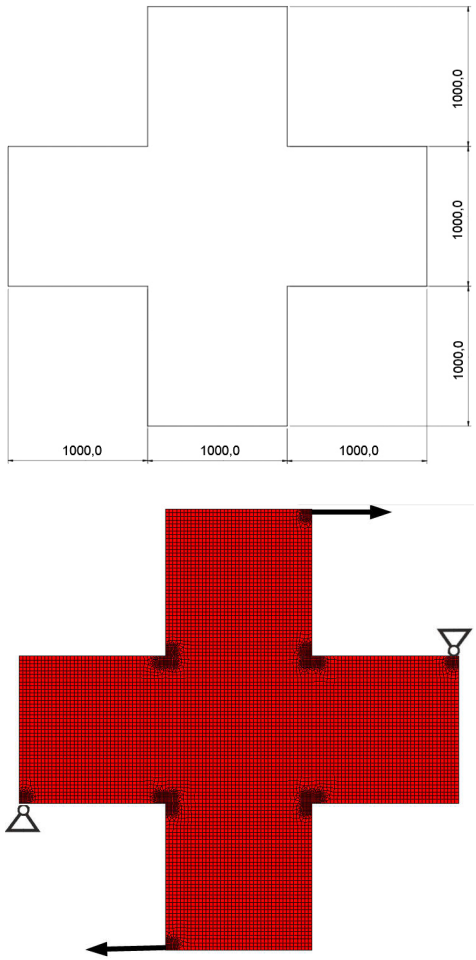

Fig. 28. The windmill structure: the structure dimensions, design domain, applied loads, and support

Table 7
The values of compliance [10^{-4} Nm] obtained while implementing the FCA algorithm for various values of β

β	0.1	6.0	8.0
Compl.	5.08	5.05	5.07

It is worth pointing out that for the examples discussed in this section the iterative process converged quickly and activation of only one reduction of the interval $[N_1, N_2]$ (after 25 iterations) was sufficient to obtain the solution. In general, the proposed unified strategy of $[N_1, N_2]$ adjustment can include a further reduction of the interval, namely, for $it > 50$ $N_1 = N \cdot 0.7$ and for $it > 75$ $N_1 = N \cdot 0.9$.

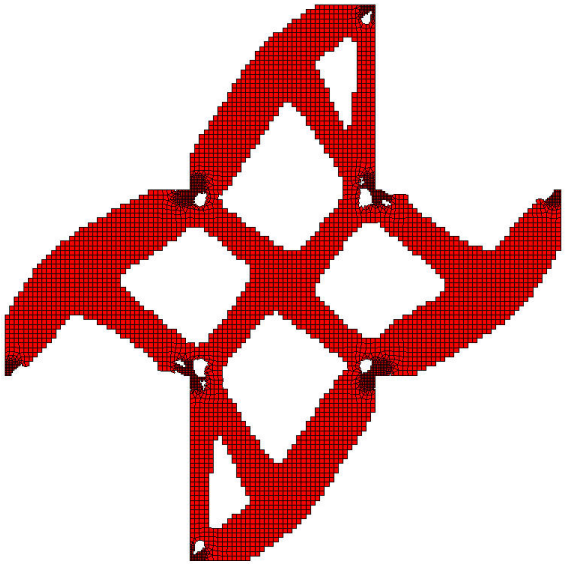

Fig. 29. Results: The final topology of the windmill structure

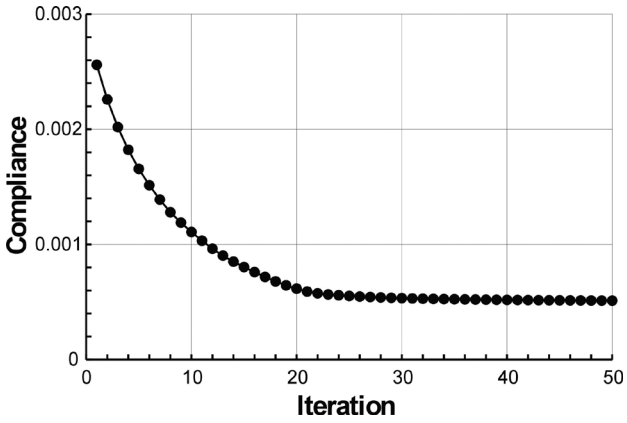

Fig. 30. Results: Compliance history for the windmill structure

6. PERFORMANCE IN 3D

In this section, a series of illustrative examples, regarding spatial structures, both under single and multiple load cases, was selected to present the effectiveness and the versatility of the proposed algorithm performance.

The same unified strategy of adjusting $[N_1, N_2]$ interval, as used in Section 5, was applied. The algorithm utilizes the von Neumann type of neighborhood for the examples of this section.

6.1. The cylindrical shell under torsion

As the first example of a spatial structure, a cylindrical shell under torsion was selected. The thickness of the shell wall is constant and equals 0.005 m, while the diameter is equal to 0.8 m. Distributed loads of 100 N are applied at selected nodes across the upper edge section, the shell is supported as shown in Fig. 31. The material data are as follows: the Young modulus $E = 210$ GPa, the Poisson ratio $\nu = 0.3$ (the material is linear, elastic, and isotropic). The supported nodes of the bottom edge of the cylinder are fixed. The regular mesh of 27720 three-dimensional 8-node elements (Solid45) was applied for a static analysis made by the ANSYS software (the element edge length: 0.01 m). The results of the structural analysis for the initial structure give a value of compliance of $7.779 \cdot 10^{-3}$ Nm. The final compliance for the volume fraction 0.5 and for $\beta = 0.1$ equals $5.909 \cdot 10^{-3}$ Nm. The final topology and the compliance history are presented in Figs. 32 and 33, respectively. Table 8 presents the values of final compliances

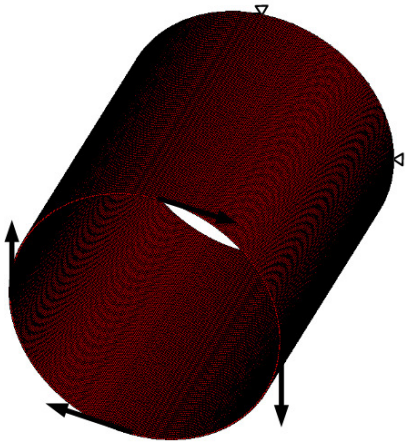

Fig. 31. Design domain, applied loads, and support

Fig. 32. Results: The final topology of the cylindrical shell

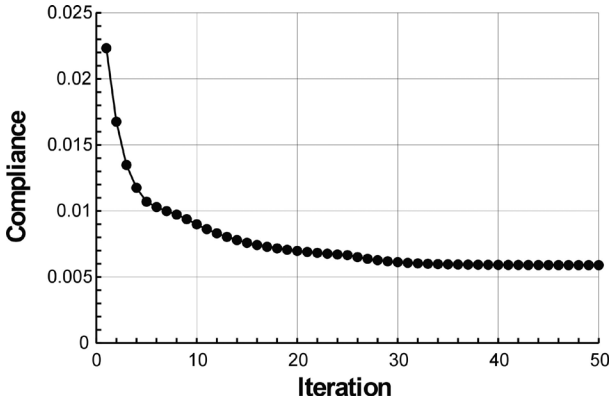

Fig. 33. Results: Compliance history for the cylindrical shell

obtained for different values of β. To make a comparison, the original CA rule of [39] was implemented to the considered structure. The resulting compliance obtained this way equals $6.323 \cdot 10^{-3}$ Nm.

Table 8
The values of compliance [10^{-3} Nm] obtained while implementing the FCA algorithm for various values of β

β	0.1	4.0	8.0
Compl.	5.91	6.30	6.51

6.2. The flange structure

The flange structure shown in Fig. 34 is considered. The structure consists of 48326 three-dimensional 8-node (Solid45) elements in mesh discretization (the element edge length: 0.002 m). The data for linear, elastic, isotropic material are: $E = 210$ GPa, $\nu = 0.3$ and volume fraction 0.5. The load of 60 kN is evenly distributed along the width of the central hole. The type of the performed analysis for the ANSYS software is static. Two cases are considered, i.e., one loading directed downward and a two-load case with downward/upward loading. The inner walls of smaller holes are fully supported, see Fig. 35.

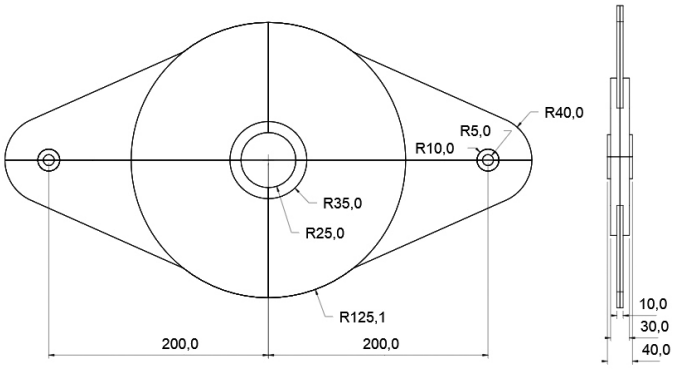

Fig. 34. The structure dimensions

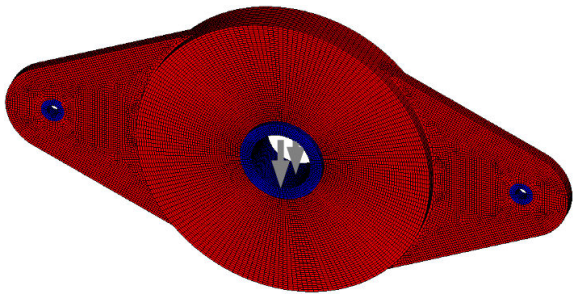

Fig. 35. An initial structure with applied loads and support

The topology generation for the single load case was performed first. Final compliance, obtained for $\beta = 4$, equals 1.734 Nm. The resulting topology together with the iteration history is presented in Figs. 36 and 37, respectively. Table 9 provides the values of final compliances obtained for different values of β. The resulting values refer to 1/4 of the structure due to the employed symmetry.

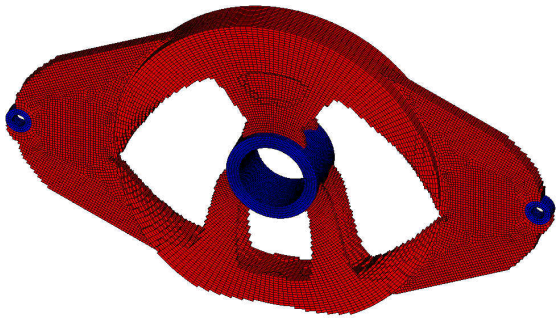

Fig. 36. Results: The final topology of the flange structure for the single load case

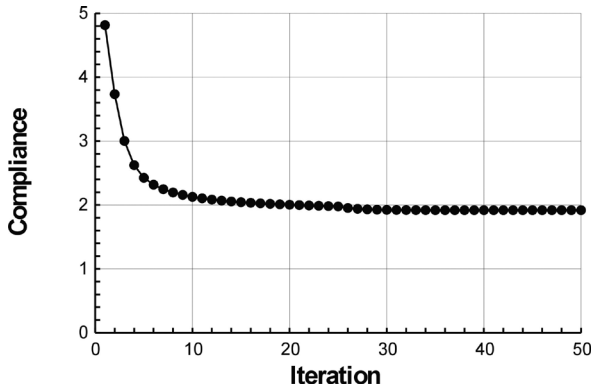

Fig. 37. Results: Compliance history for the flange structure – the single load case

Table 9
The values of compliance [Nm] obtained while implementing the FCA algorithm for various values of β

β	0.1	4.0	8.0
Compl.	1.74	1.73	1.73

It is worth noting that it is possible to extend the FCA algorithm to facilitate dealing with multiple load cases. The approach described in [3] can easily be adopted here. According to [3], equilibrium equations are solved for all load cases and the objective is defined as the sum of compliances referring to each case.

To illustrate this approach, the structure shown in Fig. 3 is revisited, and the second load, namely the vertical one acting at the upper right corner and directed upward has been added, see Fig. 38.

The topology generation has been performed for 150×150 element mesh using both the top88 algorithm [3] and the FCA one. The resulting topologies obtained for the volume fraction 0.4 are presented in Fig. 39. As can be seen from these results, the approach presented in [3] works also with the FCA algorithm.

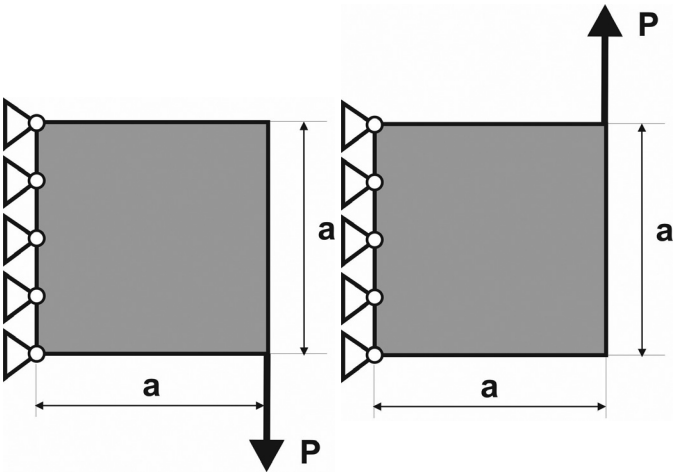

Fig. 38. The two-load case

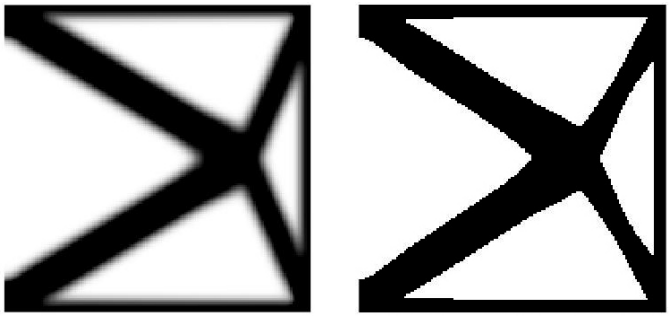

Fig. 39. The final topologies for the two-load case: [3] – left, FCA – right

The approach for the multiple-load case presented above is now applied to the flange structure considered in this section.

The topology generation has been performed and the final compliance obtained for $\beta = 0.1$ is equal to 1.918 Nm. Table 10 presents the values of the final compliances obtained for different values of β. The resulting topologies together with iteration histories are presented in Figs. 40 and 41, respectively.

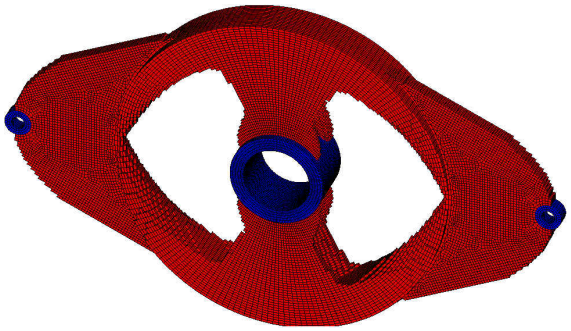

Fig. 40. Results: The final topology of the flange structure for the two-load case

Moreover, to make a comparison, the original CA rule of [43] was implemented to the above cases. The resulting compliances obtained this way equal 1.781 Nm and 1.935 Nm, respectively.

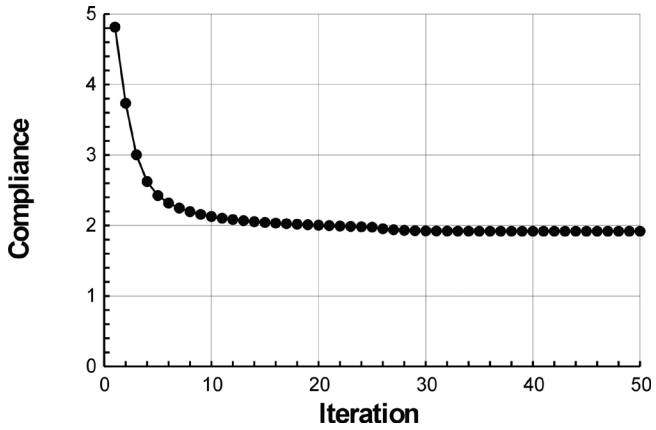

Fig. 41. Results: Compliance history for the flange structure – the two-load case

Table 10

The values of compliance [Nm] obtained while implementing the FCA algorithm for various values of β

β	0.1	4.0	8.0
Compl.	1.92	1.93	1.95

6.3. The hook structure

As the final example, a hook structure shown in Fig. 42 was selected. The thickness of the plate is equal to 4 mm. Loads of 10 kN are applied. The structure is supported along the inner walls of the bottom plate as shown in Fig. 43. The hook example was discretized with a regular mesh of 38459 three-dimensional (Solid185) elements. For the design domain, the 8-node hexahedral elements with the element edge length equal to 0.002 m and for the hook base, the tetrahedral 4-node elements were defined with the element edge length equal to 0.005 m. The Young modulus $E = 210$ GPa and the Poisson ratio $\nu = 0.3$ stand for the data of the linear, elastic, and isotropic material. The results of the structural analysis performed were applied. The result of the structural analysis for the initial structure gives the value of compliance of 46.880 Nm. The final compliance for the volume fraction is 0.35 and for $\beta = 8$ is 24.350 Nm.

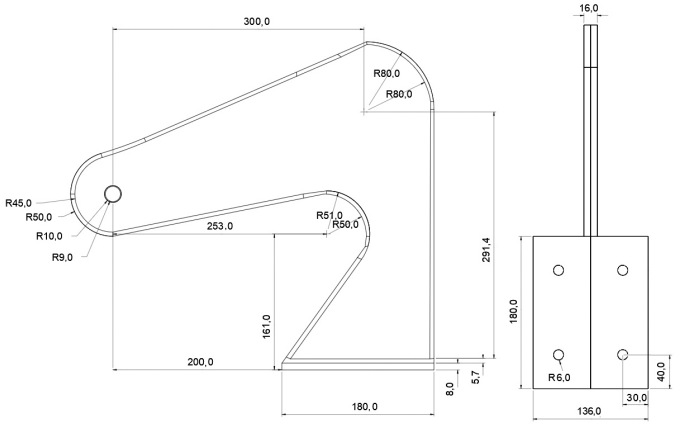

Fig. 42. The structure dimensions

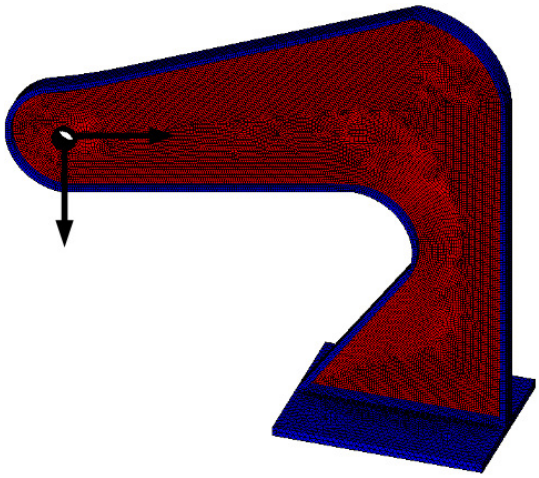

Fig. 43. Design domain, loads, and support

Table 11 presents the values of final compliances obtained for different values of β. The resulting values refer to 1/2 of the structure due to the employed symmetry. In Figs. 44 and 45, the resulting topology and iteration history are presented. The implementation of the original CA rule of [43] to the considered structure results in the compliance of 24.984 Nm.

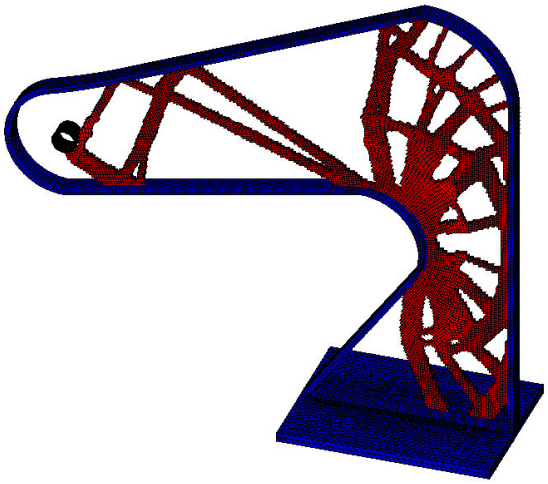

Fig. 44. Results: The final topology

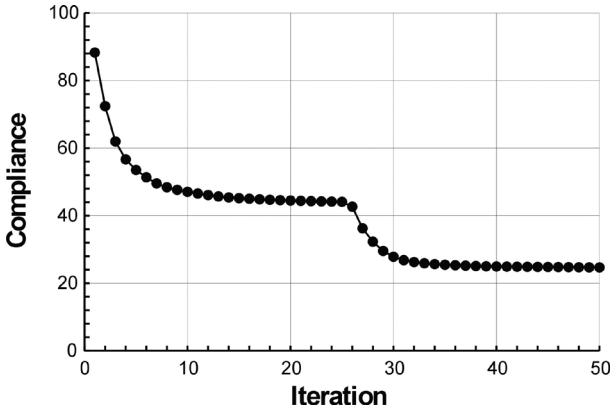

Fig. 45. Results: Compliance history

Table 11
The values of compliance [Nm] obtained while implementing the FCA algorithm for various values of β

β	0.1	4.0	8.0
Compl.	25.38	24.78	24.35

7. ABOUT THE ALGORITHM PERFORMANCE

The versatility and usefulness of the proposed approach are very important, especially from the engineering implementation point of view. Two points were considered: the strategy of adjusting $[N_1, N_2]$ interval and the β value choice.

Based on numerical tests performed (Sections 3.3 and 4), the strategy of adjusting $[N_1, N_2]$ interval is recommended, namely: one starts with $N_1 = N \cdot 0.02$ and then for $it > 25$ $N_1 = N \cdot 0.5$, for $it > 50$ $N_1 = N \cdot 0.7$ and for $it > 75$ $N_1 = N \cdot 0.9$, where N is the total number of elements. $N_2 = N \cdot 0.98$ remains unchanged for the whole iteration process. This unified strategy was applied to all engineering examples in Sections 5 and 6. It is worth pointing out that for these examples the iteration process converged quickly and only one reduction, after 25 iterations, of the interval $[N_1, N_2]$ within the above strategy was activated.

Another question to be raised is the β value choice. Usually, test calculations must be performed for small, middle, and large values to detect how they influence structure compliance. This means the selection of the function $f(n)$ between a linear one for small β, and close to step one for large β values, see Fig. 1. In the paper, the interval [0.1, 8] was adopted for the systematic β value selection. Based on the results of the tests performed and considering that the differences in the compliances obtained for the various β are not large, using an average $\beta = 4$ value as the first/basic choice can be recommended. It seems that for engineering computations this choice can also be recommended. What is worth stressing, it usually offers a better solution than the original CA algorithm [43]. Nevertheless, depending on the problem considered by selecting the β value, the solution can be further improved. Having obtained a solution for the middle value ($\beta = 4$), it is then additionally proposed to choose $\beta = 0.1$ (small) and $\beta = 8$ (large) values.

Discussing the possible automation of the topology generation process, the concept of the switching procedure can be implemented. In what follows, taking into account that the β choice is between small, middle, and large values, it is proposed to consider all of them at each iteration step. The algorithm finds a new solution for the three β values, namely, $\beta = 0.1$ (small), $\beta = 4$ (middle), and $\beta = 8$ (large), and then proceeds to the next iteration with the solution for which the compliance is the smallest one. This way the best solution can be found. To illustrate this concept the topology generation was performed for the example discussed in Section 5.1. The result is as follows, see Fig. 46.

The obtained topology is almost identical to the one presented in Fig. 26 and the compliance value equals 58.32 Nm which is close to the best solution from Table 6. It seems that the concept of the above-proposed switching technique, which is the extension of the discussed FCA algorithm, can be the subject of further research.

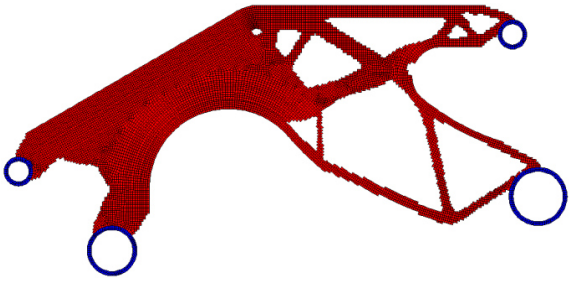

Fig. 46. The final topology obtained using the switching technique

8. CONCLUDING REMARKS

The concept of the cellular automaton based on the flexible update rules and its application to the generation of the stiffest topologies were discussed. The numerical tests of optimal topologies generation were performed for selected structures including both test examples and engineering structures. Based on the results of the performed tests, one can conclude that the proposed FCA approach allows us to obtain the final structures effectively in 2D and 3D cases. It is possible to obtain the results which have lower values of compliance as compared with the results of formerly proposed CA approaches. It is worth mentioning that one of the most important issues related to the development of a topology algorithm is the possibility of its easy implementation to solving engineering problems. The proposed algorithm is versatile and can be easily combined with any solver built on the finite element method. Since the computational cost of numerical calculations is caused mostly by the time spent on structural analyses, it is crucial to implement a sufficiently efficient structural analysis tool. The response of topological algorithm is almost immediate. Having this in mind, in this paper the efficient structural analysis module of the professional finite element system ANSYS is linked to the topology generator. Some other features worth pointing out are: the proposed algorithm does not require additional density filtering, the so-called grey elements are eliminated and generated topologies are free from the checkerboard effect.

REFERENCES

[1] M.P. Bendsoe, "Optimal shape design as a material distribution problem," *Struct. Optim.*, vol. 1, pp. 193–202, 1989.

[2] O. Sigmund, "A 99 line topology optimization code written in MATLAB," *Struct. Multidiscip. Optim.*, vol. 21, pp. 120–127, 2001.

[3] E. Andreassen, A. Clausen, M. Schvenels, B.S. Lazarov, and O. Sigmund, "Efficient topology optimization in Matlab using 88 lines of code," *Struct. Multidiscip. Optim.*, vol. 4, pp. 1–16, 2011.

[4] K. Liu and A. Tovar, "An efficient 3D topology optimization code written in Matlab," *Struct. Multidiscip. Optim.*, vol. 50, pp. 1175–1196, 2014.

[5] X.M. Xieand and G.P. Steven, *Evolutionary Structural Optimization,* Berlin: Springer, 1997.

[6] Q.M. Querin, G.P. Steven, and Y.M. Xie, "Evolutionary structural optimization using a bi-directional algorithm," *Eng. Comput.*, vol. 15, pp. 1034–1048, 1998.

[7] K. Nabaki, J. Shen, and X. Xuang, "Evolutionary topology optimization of continuum structures considering fatigue failure," *Mater. Des.,* vol. 166, pp.13, 2019.

[8] C. Kane, F. Jouveand, and M. Schoenauer, "Structural topology optimization in linear and nonlinear elasticity using genetic algorithms" in *Proc. 21st ASME Design Automatic Conference*, 1995, pp.1–8.

[9] R. Balamurugan, C. Ramakrishnan, and N. Singh, "Performance evaluation of a two stage adaptive genetic algorithm in structural topology optimization," *Appl. Soft Comput.*, vol. 8, pp. 1607–1624, 2008.

[10] H.S. Gebremedhen, D.E. Woldemichael, and F.M. Hashimi, "A firefly algorithm based hybrid method for structural topology optimization," *Adv. Model. Simul. Eng. Sci.*, vol. 7, no. 44, p. 20, 2020.

[11] A.A. Jaafer, M. Al-Bazoon, and A.O. Dawood, "Structural topology design optimization using the binary bat algorithm," *Appl. Sci*., vol. 10, no. 4, p. 1481, 2020.

[12] D. Gaweł, M. Nowak, H. Hausa, and R. Roszak, "New biomimetic approach to the aircraft wing structural design based on aeroelastic analysis," *Bull. Pol. Acad. Sci. Tech. Sci.*, vol. 65, no. 5, pp. 741–750, 2017.

[13] S.Y. Chang and S.K.Youn, "Material cloud method for topology optimization," *Numer. Methods Eng.*, vol. 65, pp. 1585–1607, 2006.

[14] H.A. Eschenauer, V.V. Kobelevand, and A. Schumacher, "Bubble method for topology and shape optimization of structures," *Struct. Optim.*, vol. 8, pp. 42–51, 1993.

[15] M.Y. Wang, X. Wang, and D. Guo, "A level set method for structural topology optimization," *Comput. Methods Appl. Mech. Eng.*, vol. 192, pp. 227–246, 2003.

[16] P. Wei, Z. Li, X. Li, and M.Y. Wang, "An 88-line MATLAB code for the parameterized level set method based topology optimization using radial basis functions," *Struct. Multidiscip. Optim.*, vol. 58, pp. 831–849, 2018.

[17] E. Biyikliand and A.C. To, "Proportional topology optimization: a new non-sensitivity method for solving stress constrained and minimum compliance problems and its implementation in Matlab," *PLoSONE*, vol. 10, pp. 1–23, 2015.

[18] Y. Xian and D.W. Rosen, "A new topology optimization approach based on Moving Morphable Components (MMC) and the ersatz material model," *Struct. Multidiscip. Optim.*, vol. 62, pp. 19–39, 2020.

[19] B. Xing and W.J. Gao, *Innovative computational intelligence: a rough guide to 134 clever algorithms*, Switzerland: Springer, 2014.

[20] T. Tarczewski, L.J. Niewiara, and L.M. Grzesiak, "Artificial bee colony based state feedback position controller for PMSM servo-drive–the efficiency analysis," *Bull. Pol. Acad. Sci. Tech. Sci.*, vol. 68, no. 5, pp. 997–1007, 2020.

[21] Y. Li and X. Wang, "Improved dolphin swarm optimization algorithm based on information entropy," *Bull. Pol. Acad. Sci. Tech. Sci.*, vol. 67, no. 4, pp. 679–685, 2019.

[22] A. Paszyńska, K. Jopek, M. Woźniak, and M. Paszyński, "Heuristic algorithm to predict the location of C^0 separators for efficient isogeometric analysis simulations with direct solvers," *Bull. Pol. Acad. Sci. Tech. Sci.*, vol. 66, no. 6, pp. 907–917, 2018.

[23] J. Von Neumann, *Theory of self-reproducing automata*, Urbana IL: University of Illinois Press, 1966.

[24] S. Ulam, "Random processes and transformations," in *Proc. International Congress of Mathematics*, 1952, vol. 2, pp. 85–87.

[25] B. Chopard and M. Droz, "Cellular automata model for the diffusion equation," *J. Stat. Phys.*, vol. 64, pp. 859–892, 1991.

[26] J.P. Crutchfield and J.E. Hanson, "Turbulent pattern bases for cellular automata," *Physica D*, vol. 69, pp. 279–301, 1993.
[27] Y. Zhao, S.A. Billings, and D. Coca, "Cellular automata modelling of dendritic crystal growth based on Moore and von Neumann neighborhoods," *Int. J. Model. Identif. Control*, vol. 2, no. 6, pp. 119–25, 2009.
[28] P. Rosin, A. Adamatzky, and X. Sun (eds.), *Cellular Automata in Image Processing and Geometry*, Switzerland: Springer International Publishing, 2014.
[29] N. Inou, N. Shimotai, and T. Uesugi, "A cellular automaton generating topological structures," in *Proc. 2nd European Conference on Smart Structures and Materials*, 1994, vol. 2361, pp. 47–50.
[30] N. Inou, T. Uesugi, A. Iwasaki, and S. Ujihashi, "Self-organization of mechanical structure by cellular automata," *Key Eng. Mater.*, vol. 145–149, pp. 1115–1120, 1998.
[31] E. Kita and T. Toyoda, "Structural design using cellular automata," *Struct. Multidiscip. Optim.*, vol. 19, pp. 64–73, 2000.
[32] P. Hajela and B. Kim, "On the use of energy minimization for CA based analysis in elasticity," *Struct. Multidiscip. Optim.*, vol. 23, pp. 24–33, 2001.
[33] B. Tatting and Z. Gurdal, "Cellular automata for design of two-dimensional continuum structures," in *Proc. 8th AIAA/USAF/NASA/ISSMO Symposium on Multidisciplinary Analysis and Optimization*, 2000, p. 10.
[34] S. Missoum, Z. Gurdal, and S. Setoodeh, "Study of a new local update scheme for cellular automata in structural design," *Struct. Multidiscip. Optim.*, vol. 29, pp. 103–112, 2005.
[35] M.M. Abdalla and Z. Gurdal, "Structural design using cellular automata for eigenvalue problems," *Struct. Multidiscip. Optim.*, vol. 19, pp. 64–73, 2004.
[36] B. Hassani and M. Tavakkoli, "A multi-objective structural optimization using optimality criteria and cellular automata," *Asian J Civ. Eng. Build. Hous.*, vol. 8, pp. 77–88, 2007.
[37] C.L. Penninger, A. Tovar, L.T. Watson, and J.E. Renaud, "KKT conditions satisfied using adaptive neighboring in hybrid cellular automata for topology optimization," in *Proc. 8th World Congress on Struct. Multidiscip. Optim.*, 2009, p. 10.
[38] J. Jia *et al.*, "Multiscale topology optimization for non-uniform microstructures with hybrid cellular automata," *Struct. Multidiscip. Optim.*,vol. 62, pp. 757–770, 2020.
[39] M. Afrousheh, J. Marzbanrad, and D. Gohlich, "Topology optimization of energy absorbers under crashworthiness using modified hybrid cellular automata (MHCA) algorithm," *Struct. Multidiscip. Optim.*, vol. 60, pp. 1021–1034, 2019.
[40] A. Tovar, N.M. Patel, and A.K. Kaushik, "Hybrid cellular automata: a biologically-inspired structural optimization technique," in *Proc. 10th AIAA/ISSMO Multidisciplinary Analysis and Optimization Conference*, 2004, p.15.
[41] A. Tovar, N.M. Patel, G.L. Niebur, M. Sen, and J.E. Renaud, "Topology optimization using a hybrid cellular automaton method with local control rules," *J. Mech. Des.*, vol. 128, pp. 1205–1216, 2006.
[42] C.L. Penninger, A. Tovar, L.T. Watson, and J.E. Renaud, "KKT conditions satisfied using adaptive neighboring in hybrid cellular automata for topology optimization," *Int. J. Pure Appl. Math.*, vol. 66, pp. 245–262, 2011.
[43] B. Bochenek and K. Tajs-Zielinska, "Novel local rules of Cellular Automata applied to topology and size optimization," *Eng. Optim.*, vol. 44, pp. 23–35, 2012.
[44] B. Bochenek and K. Tajs-Zielinska, "Topology optimization with efficient rules of cellular automata," *Eng. Comput.*, vol. 30, pp. 1086–1106, 2013.
[45] B. Bochenek and K. Tajs-Zielinska, "Minimal compliance topologies for maximal buckling load of columns," *Struct. Multidiscip. Optim.*, vol. 51, pp. 1149–1157, 2015.
[46] B. Bochenek and K. Tajs-Zielinska, "GOTICA – generation of optimal topologies by irregular cellular automata," *Struct. Multidiscip. Optim.*, vol. 55, pp. 1989–2001, 2017.
[47] M.P. Bendsoe and N. Kikuchi, "Generating optimal topologies in optimal design using a homogenization method," *Comput. Methods Appl. Mech. Eng.*, vol. 71, pp. 197–224, 1988.
[48] J. Lim, C. You, and I. Dayyani, "Multi-objective topology optimization and structural analysis of periodic spaceframe structures," *Mater. Des.*, vol. 190, pp.16, 2020.
[49] P. Gomes and R. Palacios, "Aerodynamic-driven topology optimization of compliant airfoils," *Struct. Multidiscip. Optim.*, vol. 62, pp. 2117–2130, 2020.
[50] J. Wu and J. Wu, "Revised level set-based method for topology optimization and its applications in bridge construction," *Open Civ. Eng. J.*, vol. 11, pp. 153–166, 2017.
[51] A.J. Muminovic, M. Colic, E. Mesic, and I. Saric, "Innovative design of spur gear tooth with infill structure," *Bull. Pol. Acad. Sci. Tech. Sci.*, vol. 68, no. 3, pp. 477–483, 2020.
[52] L.L. Beghini, A. Beghini, N. Katz, W.F. Baker, and G.H. Paulino, "Connecting architecture and engineering through structural topology optimization," *Eng. Struct.*, vol. 59, pp. 716–726, 2014.
[53] K. Tajs-Zielinska and B. Bochenek, "Topology optimization – engineering contribution to architectural design," *IOP Conf. Ser.: Mater. Sci. Eng.*, vol. 245, pp.10, 2017.
[54] F. Regazzoni, N. Parolini, and M. Verani, "Topology optimization of multiple anisotropic materials, with application to self-assembling diblock copolymers," *Comput. Methods Appl. Mech. Eng.*, vol. 338, pp. 562–596, 2018.
[55] S. Das and A. Sutradhar, "Multi-physics topology optimization of functionally graded controllable porous structures: Application to heat dissipating problems," *Mater. Des.*, vol. 193, pp.13, 2020.
[56] M.P. Bendsoe and O. Sigmund, *Topology optimization. Theory, methods and applications,* Berlin Heidelberg New York: Springer, 2003.
[57] O. Sigmund and K. Maute, "Topology optimization approaches," *Struct. Multidiscip. Optim.*, vol.48, pp. 1031–1055, 2013.
[58] J.D. Deaton, and R.V. Grandhi, "A survey of structural and multidisciplinary continuum topology optimization: post 2000," *Struct. Multidiscip. Optim.*, vol. 49, pp. 1–38, 2014.
[59] J. Liu *et al.*, "Current and future trends in topology optimization for additive manufacturing," *Struct. Multidiscip. Optim.*, vol. 57, pp. 2457–2483, 2018.
[60] M.A. Herfelt, P.N. Poulsen, and L.C. Hoang, "Strength-based topology optimization of plastic isotropic von Mises materials," *Struct. Multidiscip. Optim.*, vol.59, pp. 893–906, 2019.
[61] B. Błachowski, P. Tauzowski, and J. Lógó, "Yield limited optimal topology design of elastoplastic structures," *Struct. Multidiscip. Optim.*, vol.61, pp. 1953–1976, 2020.
[62] L. Xia, F. Fritzen, and P. Breitkopf, "Evolutionary topology optimization of elastoplastic structures," *Struct. Multidiscip. Optim.*, vol. 55, pp. 569–581, 2017
[63] B. Bochenek and M. Mazur, "A novel heuristic algorithm for minimum compliance optimization," *Eng. Trans.*, vol. 64, pp. 541–546, 2016.